Convective Squalls over the Eastern Equatorial Atlantic

FLORIAN BERKES

Johannes Gutenberg University Mainz, Mainz, Germany

PETER KNIPPERTZ AND DOUGLAS J. PARKER

University of Leeds, Leeds, United Kingdom

GUS JEANS

Fugro, Wallingford, United Kingdom

VALÉRIE QUINIOU-RAMUS

TOTAL S.A, Paris, France

(Manuscript received 25 July 2011, in final form 23 January 2012)

ABSTRACT

The Congo Basin and the adjacent equatorial eastern Atlantic are among the most active regions of the world in terms of intense deep moist convection, leading to frequent lightning and severe squalls. Studying the dynamics and climatology of this convection is difficult due to a very sparse operational network of ground-based observations. Here, a detailed analysis of recently available high temporal resolution meteorological observations from three oil platforms off the coast of Angola spanning the three wet seasons from 2006/07 to 2008/09 is presented. The annual cycle of squall days as identified from wind data closely follows that of convective available potential energy (CAPE) and therefore mirrors the cycle of wet and dry seasons. The diurnal cycle of squall occurrence varies from station to station, most likely related to local features such as coastlines and orography, which control the initiation of storms. An attempt to classify squalls based on the time evolution of the station meteorology and satellite imagery suggests that microbursts account for at least one-third of the strong gusts, while mesoscale squall lines appear to be quite rare. On a daily basis the probability of squall occurrence increases with increasing values of CAPE, downdraft CAPE, and 925–700-hPa wind shear, and decreases for high convective inhibition, all calculated from vertical profiles of temperature and humidity at the nearest grid point in the NCEP–NCAR and ECMWF reanalysis datasets. Both the climatological results and the stability indices can be used for local forecasting to avoid squalls impacting on operations on the offshore platforms.

1. Introduction

The Congo Basin is one of the two major tropical continental zones of active convection (the other being the Amazon Basin), characterized by extensive rain forest and intense lightning activity (Toracinta and Zipser 2001; Christian et al. 2003; Williams and Sátori 2004). Despite its importance for the global circulation (Jury et al. 2009), energy and water budgets, and the global electrical circuit, the scarcity of ground-based observations hampers a detailed analysis of the dynamics and climatology of convective systems in this region. The few existing studies rely largely on satellite data (e.g., Laing and Fritsch 1993; McCollum et al. 2000; Nguyen and Duvel 2008; Jackson et al. 2009; Laing et al. 2011). To the best of our knowledge, there are currently no operational forecasts for severe convection for this region, despite the fact that convective squalls can pose a substantial threat inland, and to shipping and oil platforms over the adjacent eastern equatorial Atlantic Ocean. A good observational network is needed to monitor local triggers of convection such as orographic features and land or sea breezes, which often create distinct diurnal cycles (Jackson et al. 2009; Laing et al. 2011), and to understand the influence of seasonal changes in sea surface

Corresponding author address: Florian Berkes, Johannes Gutenberg University Mainz, Becherweg 21, 55099 Mainz, Germany. E-mail: berkesf@uni-mainz.de

DOI: 10.1175/WAF-D-11-00086.1

temperatures and regional circulation systems (McCollum et al. 2000; Leroux 2001; Yang and Slingo 2001; Mori et al. 2004; Balas et al. 2007), and of equatorial wave phenomena such as the Madden–Julian oscillation (Nguyen and Duvel 2008; Laing et al. 2011).

There is an extensive body of literature from other parts of the world on the generation of severe squalls by intense convective systems. Key to all types is the descent of cool air in a ''downdraft'' caused by melting, sublimation, and evaporation of hydrometeors, which can be enhanced through precipitation drag (Knupp and Cotton 1985; Proctor 1988, 1989; Wakimoto 2001). When these downdrafts hit the ground, they spread horizontally as ''cold pools'' and produce strong surface squalls. Short-lived small-scale (few kilometers) events are usually related to so-called microbursts (Proctor 1989; Doswell 2001), while mesoscale organization of convection can lead to several hundred kilometer long squall lines and extensive cold pools (Houze 1977; Zipser 1977; Chong et al. 1987). The passage of the leading edge of a mesoscale cold pool is usually associated with coherent changes in wind speed and direction, a temperature decrease, and a pressure jump. Abrupt changes in humidity are often observed, too, but these can be negative or positive depending on the ambient conditions and depth of the downdraft. Precipitation associated with a squall line typically starts with a marked band of heavy downpours shortly after the passage of the leading edge, followed by more moderate stratiform rains that can last for several hours.

The need to quantify, characterize, and forecast squalls has motivated several observational programs in the waters offshore of western equatorial Africa over recent years by the oil and gas industry. This study is the first to present a detailed climatological and dynamical analysis derived from these unique data. The goal of this study is to explore different ways of providing guidance for severe squall warning. Section 2 provides background on the data used in this study. Section 3 contains a climatological analysis of squall days followed by an attempt to characterize these days based on surface and satellite measurements in section 4. Section 5 investigates the relationship between squall occurrence and classical instability indices on a monthly and daily basis. A short summary and discussion are presented in the concluding section 6.

2. Data

The central dataset used for this paper contains meteorological observations from three oil platforms offshore of the western coast of equatorial Africa provided by the West African Gust (WAG) project phase 3 coordinated by Fugro GEOS Ltd. These platforms are

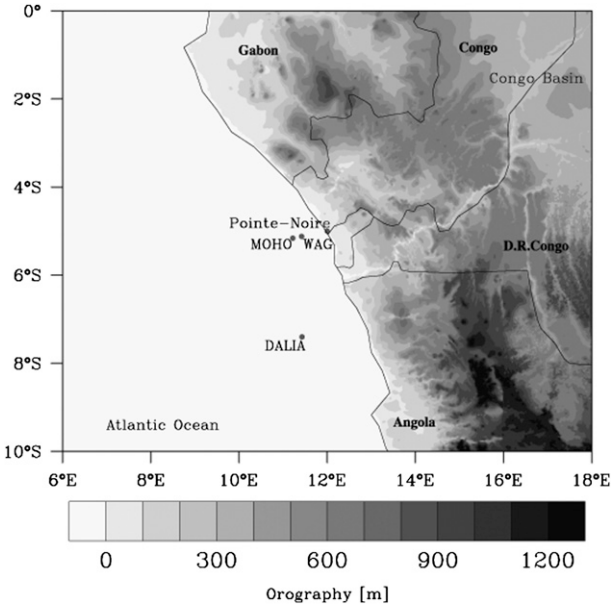

FIG. 1. Topography of the study region with geographical names used in the text and the locations of the three oil platforms (WAG, MOHO, and DALIA) that provided data for this study.

located at 05°12′S, 11°42′E (referred to as WAG hereafter), at 05°16′S, 11°22′E (MOHO), and at 07°40′S, 11°43′E (DALIA; see Fig. 1 for locations). WAG and MOHO are located to the west of the Angolan enclave Cabinda, about 40 km from the coast for WAG and almost 80 km for MOHO. DALIA is about 160 km west of the coast of northern Angola. DALIA provided continuous measurements for the period from January 2007 to March 2009. Measurements at WAG cover 1 January–23 May 2007 and 3 December 2007–17 July 2008, while MOHO was only active during 28 May 2008–31 March 2009. As shown by Jackson et al. (2009), hardly any mesoscale convective systems (MCSs) occur outside of the rainy season of November–May. With this in mind the dataset covers three such rainy seasons (2006/07, 2007/08, and 2008/09), with the November and December of the first season and the May and April of the last season missing. Due to the proximity of WAG and MOHO, a climatology for the northern region can be constructed by using data from the former for the first two seasons and from the latter for 2008/09. This way, the data coverage practically equals that of DALIA.

Parameters used for this study are wind speed and direction measured at 38 m MSL, air temperature and relative humidity measured at 30 m MSL, as well as pressure measured at 17 m MSL. Conversion from relative to specific humidity was done with the method discussed in Bolton (1980). The wind measurements are taken using a mast that extends some 15 m above the actual oil platform

and should therefore not be strongly influenced by its presence. All measurements are taken every second and are then averaged over 1 min. In addition, precipitation from an automatic rain gauge manufactured by Observator Instruments is available for 1-min, 10-min, and 1-h intervals.

Extensive quality control was applied to the large volume of measured data in several distinct stages. Preliminary quality control included conversion of wind directions to degrees true and the removal of invalid records at the start and end of each measurement period. All 1-s data were then subjected to careful spike removal, following objective assessment of all apparent spikes. As the primary application was the quantification of the squall wind structure, more attention was paid to wind speeds than any other parameter. Wind direction sensor alignment corrections were also applied at this stage, in addition to temperature, pressure, and humidity offsets following calibration checks. There followed a meticulous examination of sheltering and other platform structural effects. This was ultimately supported by wind tunnel modeling, as described by Jeans and Johnson (2011). Finally, 1-min scalar mean speeds and unit vector mean directions were calculated from 1-s data, after the removal of structurally contaminated records. Time series corresponding to each identified squall were then extracted for further analysis.

Data of this quality and resolution are extremely rare in this part of the tropics and can therefore give important first insights into the convective regime in this area despite the relatively short time series available. It is worth noting that like data from research ships, these observations enable a true assessment of conditions over the ocean, while recordings even from small islands will always be to some extent influenced by the different thermodynamic and roughness characteristics of the land. Unlike ship data, the measurements used here have the advantage of long time series at a set of fixed points.

In addition to these observations, standard infrared (IR; 10.8-μm channel) images from the geostationary *Meteosat-9* at 15-min temporal resolution have been used for identification, classification, and tracking of convective systems affecting the three oil platforms. To aid this process 3-hourly rain rates from the Tropical Rainfall Measuring Mission (TRMM) and Other Rainfall Estimate (3B42 V6; Huffman et al. 2007) were obtained from the National Aeronautics and Space Administration (NASA) online Giovanni system. These precipitation estimates are derived by a combination of TRMM's rainfall radar with microwave and IR products using monthly gauge-based calibration techniques. Significant gaps in the microwave and radar satellite swaths reduce the reliability of the product on short time scales (Negri et al. 2002). Atmospheric data were taken from the National Centers for Environmental Prediction–National Center for Atmospheric Research (NCEP–NCAR) 40-Year Reanalysis project (Kalnay et al. 1996) on standard pressure levels with 2.5° horizontal grid spacing. To check for the robustness of our results, parts of the analysis were repeated with European Centre for Medium-Range Weather Forecasts (ECMWF) Interim Re-Analysis (ERA-Interim) data (Dee et al. 2011). We also compared vertical profiles of temperature and humidity to the nearest radiosonde station, Pointe Noire (see Fig. 1), which conducted 156 launches during the three rainy seasons considered here. The investigations focus on 0000 UTC data as a representation of conditions for convection on the following day, but other times will be discussed, too.

3. Climatology

a. Identification, geographical distribution, and interannual variability

Squall events were objectively identified based on the widely used definition by the World Meteorological Organization (WMO 1962): ''A sudden increase of wind speed by at least 8 m s^{-1}, rising to 11 m s^{-1} or more and lasting for at least one minute.'' Sudden is not defined in exact terms here and was chosen to be within no more than 10 min for this study. Note that this definition is usually applied to winds at 10 m above ground. The higher elevation of the measurements employed here implies that somewhat weaker squalls can fulfill the WMO definition. A total number of 61 individual events were identified. On 7 days two squalls were identified at the same station. As it appeared to be rather difficult to determine whether these are related to clearly separable weather systems, it was decided to count these as one event with the higher wind speed occurrence retained. This leads to a reduction to a total of 54 events: 32 at WAG, 9 at MOHO, and 13 at DALIA.

These numbers are to some extent a reflection of the different periods for which data are available (see section 2). However, they also indicate a general tendency for more squall activity at the northern stations (41 in total) than at DALIA, which is consistent with the MCS climatology by Jackson et al. (2009, their Fig. 2a). Another reason for this difference is probably the longer distance from DALIA to the coast and therefore the reduced influence of sea- or land-breeze processes or convective triggers over land. This is again consistent with the MCS climatology by Jackson et al. (2009), which shows a very sharp dropoff of organized convective activity along the coast between 5° and 15°S. Comparing the two neighboring stations, WAG and MOHO,

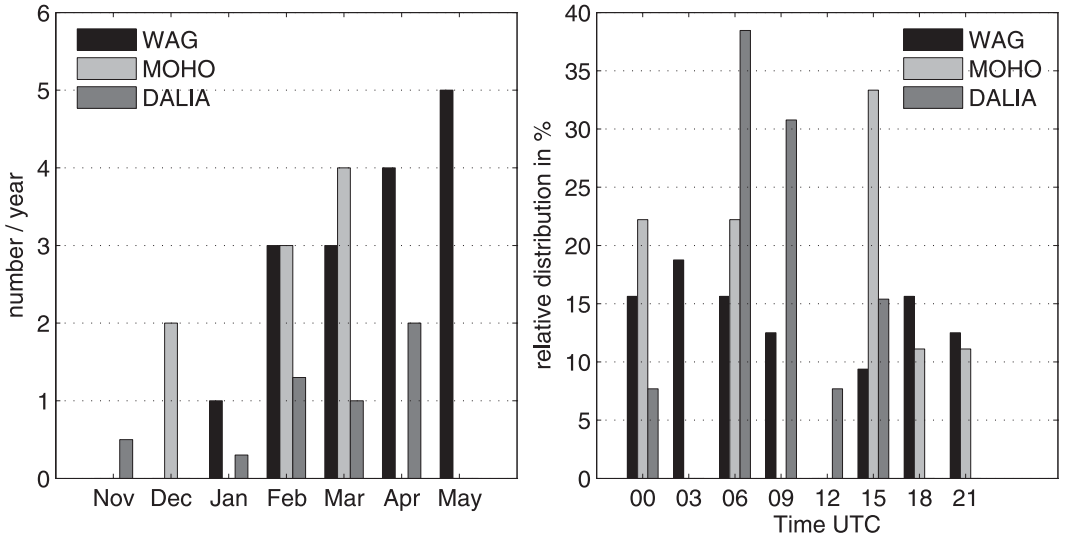

FIG. 2. Climatology of squall days at WAG (black), MOHO (light gray), and DALIA (dark gray). (left) Distribution of average monthly values. January, February, and March are available for the years 2007–09. The other months are available for only 2 yr (see section 2 for details). (right) Diurnal distribution in % for 3-hourly intervals starting with 0000–0300 UTC.

is difficult, because no data are available for the most active months (April and May) at the latter station. Nevertheless, the reduced squall occurrence at MOHO could also be a reflection of the rapid decay of severe convection over the ocean. Total numbers from all available stations per rainy season indicate somewhat less activity in 2007/08 (complete data coverage) than in 2006/07 (weakly active months of November and December missing) and in 2008/09 (most active months of April and May missing). Such variations could be related to changes in local sea surface temperatures, as investigated by Balas et al. (2007).

b. Annual and diurnal cycle

Figure 2a shows the average monthly distribution of squall days for WAG, MOHO, and DALIA. As no squalls occurred outside of the rainy season, only the period from November to May is displayed. This is a clear indication that all high-wind events under study here are related to precipitation processes in connection with the southward migration of the intertropical convergence zone (ITCZ) rather than dry dynamical effects due to orography, for example. Very stable atmospheric conditions associated with coastal upwelling and the cold waters of the Benguela Current to the southwest usually dominate the dry season in this region. The first 3 months of the rainy season (November–January) are characterized by very sporadic squall events at all three stations (Fig. 2a). Cold clouds and MCSs are strongly confined to the land during this period (Jackson et al. 2009; Laing et al. 2011). The statistics are clearly dominated by the core of the main rainy season from February to May with three or more events per month at WAG. MOHO shows similar numbers of squalls in February and March as WAG, but unfortunately there are no data from MOHO in April and March. DALIA has maximum activity in February–April, but shows a dropoff in May when the ITCZ starts moving northward.

The diurnal cycle of tropical convection is an important feature in our understanding of the dynamics of initiation, organization, and propagation in the absence of synoptic-scale controls (e.g., Yang and Slingo 2001). The southern DALIA station shows a very distinct morning peak, with maximum activity between 0600 and 1200 UTC (dark gray bars in Fig. 2b). Note that local time is UTC + 1 h. Squall occurrence quickly falls off toward the afternoon and early morning hours, with no activity at all from 1800 UTC until midnight. According to a χ^2 test, this diurnal pattern is distinct from a random distribution above the 95% confidence level. It is consistent with a formation of convection over land in the afternoon and evening hours (see Jackson et al. 2009), possibly in connection with the sea-breeze convergence or orographic effects (see Fig. 1), and a subsequent propagation out over the ocean. Such a pattern of behavior was evident in satellite imagery for some squall cases (not shown; see Laing et al. 2011) and has been observed for other tropical regions such as Indonesia (Mori et al. 2004). It offers a possible explanation for the smaller number of squalls at DALIA: only systems that are well enough organized to propagate some 200 km

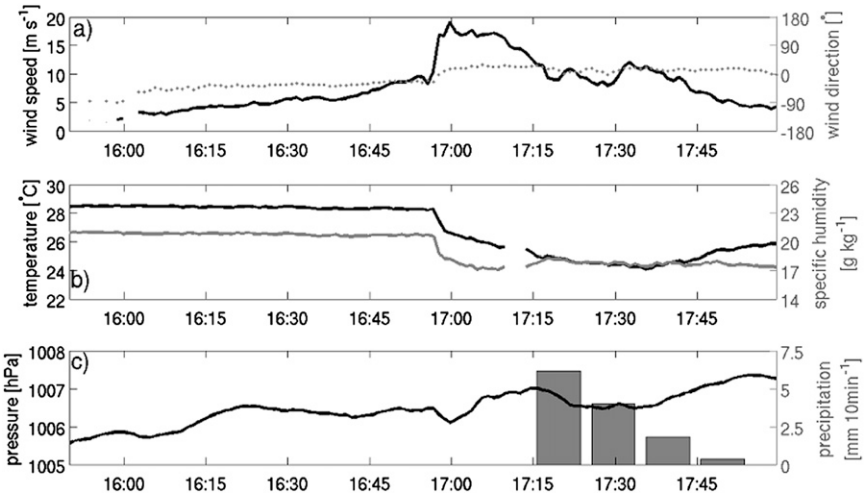

FIG. 3. Squall-line passage at WAG observed between 1600 and 1800 UTC 24 Mar 2007. (a) Wind speed and direction, (b) temperature and specific humidity, and (c) pressure and precipitation. All values but precipitation are 1-min means.

across the ocean cause squalls here. These will be rarer than shorter-lived, more localized storms, more of which may affect WAG and MOHO.

The diurnal cycle at the northern stations is more difficult to interpret. At WAG (black bars in Fig. 2b), most squalls occur during the early morning hours between 0000 and 0600 UTC followed by a marked drop around midday. A secondary maximum is observed at 1800 UTC. MOHO (light gray bars in Fig. 2b) also shows enhanced activity during the second half of the night and in the afternoon, but the small number of cases makes is hard to interpret any details. Both stations are not significantly different from a random distribution according to a χ^2 test. The same holds for the diurnal cycle resulting from combining observations from WAG and MOHO. Generally, the shift toward an earlier maximum than at DALIA is consistent with the shorter distance from the coast, assuming longer-lived, organized systems triggered over land. The afternoon activity is more difficult to understand and could be the result of more short-lived localized events or very long-lived systems that have propagated from much farther inland. Both cases were observed with satellite data. The following section will present an example for a long-lived system.

4. Classification

To better understand the dynamical behavior of the observed squall events, a classification has been attempted based on the available station observations and satellite data. An example of a mesoscale squall line on 24 March 2007 is given in Figs. 3 and 4. The system hit the WAG oil platform around 1700 UTC with 1-min mean wind speeds of almost 20 m s^{-1}, increasing rapidly from 7–8 m s^{-1} in just a few minutes (Fig. 3a). The wind direction changed from NNW to NNE with the arrival of the squall. Wind speeds then decreased gradually to about 4 m s^{-1} around 1 h after the passage, indicating a spatially extended cold pool. Temperature decreased from a very stable 28.5°C to about 24°C in just above half an hour with a marked drop at the leading edge (Fig. 3b). The specific humidity shows a marked drop from about 20 to 17 g kg^{-1} with the arrival of the squall, most likely related to downdrafts of drier air from aloft (see McCollum et al. 2000). The onset of precipitation occurred around 1715 UTC (Fig. 3c). The rainfall continued for less than 40 min, accumulating to about 12 mm with decreasing intensity. While the latter fits classical ideas of squall lines with a sharp leading edge and a trailing stratiform region, the duration of the event is quite short. The pressure shows a slight decrease with the arrival of the leading edge followed by an increase of about 0.8 hPa (Fig. 3c). During the precipitation period, another slight decrease and an increase are observed. Overall, these fluctuations are rather weak compared to squall lines described in the literature (e.g., Chong et al. 1987). Nevertheless, satellite imagery suggests a line organization of the system with cold cloud tops from the coast of Gabon to northern Angola over a length of about 750 km (Fig. 4a). The TRMM rainfall product indicates several cells with intensities of more than 10 mm h^{-1} embedded in the line (Fig. 4b), but none of these tracked across the WAG station (only 4 mm h^{-1} on average during 1500–1800 UTC). Both IR imagery and TRMM precipitation data indicate a southwestward propagation (not shown), roughly consistent with the shift to NNE winds at WAG.

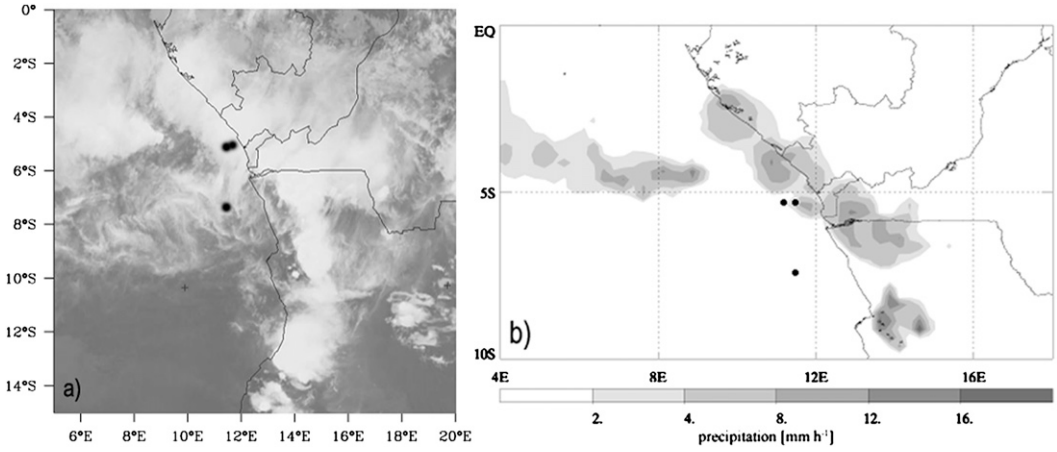

FIG. 4. Squall line on 24 March as observed from space. (a) Meteosat 10.8-μm channel for 1658 UTC and (b) TRMM precipitation rate in mm h^{-1} for 1500–1800 UTC. Political borders and the locations of the three oil platforms are marked.

Based on the inspection of single squall events like the one discussed above, a set of criteria was put together to distinguish between larger-scale, more organized squall lines and small, shorter-lived microbursts for the entire dataset (see Table 1 for details). These criteria loosely follow experiences from regions with a much better database of information on convective squalls, such as the United States (Doswell 2001). Unfortunately, 30 of the squall cases (56%) could not be assigned to either of the two categories with sufficient confidence and were therefore termed unclassified (Fig. 5). There are a number of reasons for this rather disappointing result. (i) Given the rather limited set of information available, we preferred to be conservative about the classification and to only assign a system to a given type, when we had robust reasons based on surface and satellite observations. Consequently, it is quite possible that some of the ''unclassified'' events would fall into either of the two categories, had we had the data to make a better judgment. (ii) Interpretation of satellite information was often not straightforward due to extensive cirrus cover and uncertainties in the TRMM rainfall on short time scales (Negri et al. 2002). (iii) Given that the surface stations are at the very margin of the MCS activity over the continent (Jackson et al. 2009), some events might be related to decaying systems or systems undergoing a transition to more oceanic conditions, such that they do not show stereotypical patterns anymore. Overall, the ''unclassified'' cases show a wide range in their behavior that can hardly be documented or summarized here.

Among the classified cases, 18 (1/3 of all and 3/4 of all classified systems) appear to be of the microburst type, with at least one occurrence at all three stations. Only six proper squall lines could be identified with some confidence, all of which occurred at the northern two stations. This is somewhat surprising as the diurnal cycle at the DALIA station suggests a propagation of longer-lived, more organized systems from the land (section 3b). Again, the decay of systems over the ocean or small-scale structures within them might make it difficult to properly classify them. A possible reason for the general lack of clearly identifiable squall lines might be the deeper moist column in this part of the tropics during the rainy season [e.g., compared to the Sahel; see McCollum et al. (2000)], which reduces the evaporation of precipitation, as well as a moderate vertical wind shear (Laing et al. 2011; see also discussion in Williams and Sátori 2004).

TABLE 1. Subjective criteria used to classify the observed squalls into different types, loosely based on work by Doswell (2001) and Chong et al. (1987).

	Squall line	Microburst
Wind speed	Sudden increase followed by slow gradual decrease	Short spike
Temperature	Substantial, prolonged decrease	Short decrease
Pressure	Short jump	Variable
Precipitation	Some delay to squall, heavy at first, then more moderate	Shortly after or concomitant with squall
IR images	Convective line with several hours lifetime	Single or multiple cells, less organization, shorter lifetime
TRMM	Precipitation over larger area	Precipitation more localized

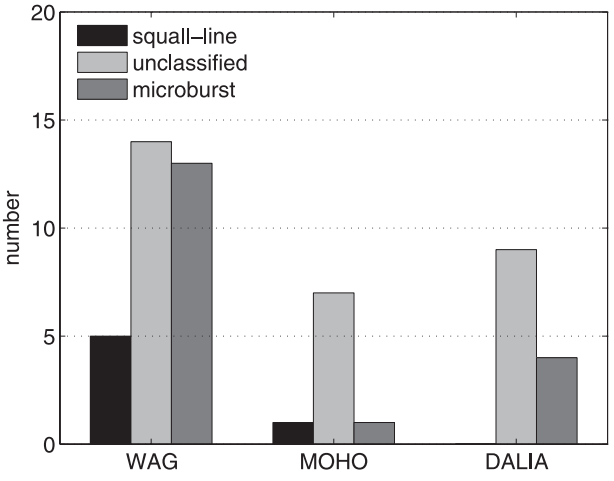

FIG. 5. Classification of squall days for the oil platforms WAG, DALIA, and MOHO according to the legend in the top-left corner. The criteria for this classification are given in Table 1 and are discussed in section 4.

5. Stability indices

A possible approach to a better physical understanding of the observed squalls that might lead to improved forecasts is the use of stability indices (Müller et al. 1993; Rasmussen and Blanchard 1998; Savvidou et al. 2010). Marsham et al. (2008) used such indices successfully, based on ECMWF model analysis data over the West African Sahel, to describe the seasonal evolution of squall winds in this inland region. The following subsections will give a short introduction to the indices used (section 5a), followed by monthly climatologies (section 5b), day-to-day relationships between the indices and the occurrence of squalls (section 5c), and a comparison between NCEP and ECMWF data (section 5d).

a. Index definitions and data

Mathematical definitions for the indices used here are given in the appendix. Here, only a brief introduction of their meaning is provided.

(i) Convective available potential energy (CAPE) is the most fundamental measure of cumulonimbus energy (Emanuel 1994) and is based on the integral of the cloud buoyancy from the level of free convection (LFC) to the level of neutral buoyancy (LNB). In other words, CAPE is the thermodynamic energy that can potentially be used for the vertical acceleration of a convecting parcel of air once it reaches the LFC.

(ii) Convective inhibition (CIN) is defined in a similar way, but restricting the integral to the negatively buoyant layer below the LFC. CIN is therefore the energy needed to lift an air parcel to the point where it becomes buoyant and can then rise freely. CIN can be overcome through near-surface convergence caused by orographic features or land–sea circulations. Increasing the equivalent potential temperature (θ_e) of the near-surface air leads to increasing CAPE and reducing CIN (e.g., Emanuel 1994) and, therefore, a negative correlation between the two (see section 5c). CIN and CAPE were set to zero for profiles without a discernible LFC.

(iii) For the computation of downdraft CAPE (DCAPE), it is assumed that an air parcel is isobarically cooled to its wet-bulb temperature and then descends to the surface with its state of saturation being maintained by evaporation throughout the process (Emanuel 1994). DCAPE can be understood to be a measure of the maximum possible energy available to a convective downdraft (although it does not take into account the weight of precipitation). Consequently, it is often closely related to the strength of the surface squall winds associated with deep convection. It is computed as a vertical integral of the negative buoyancy of an air parcel starting form a given pressure level downward to the surface. Here, we chose to use the pressure level giving the highest DCAPE value. Both CAPE and DCAPE strongly depend on the temperature lapse rate and therefore tend to correlate positively (see sections 5b and 5c). The realization of DCAPE depends on interactions between convective clouds and ambient air such as entrainment or hydrometeors falling into unsaturated subcloud layers.

(iv) Vertical wind shear in the lower troposphere plays an important role in separating downdrafts and updrafts in deep moist convection with important ramifications for convective organization, particularly into long-lived squall lines. It is represented here by the magnitude of the vector difference between 925 and 700 hPa (referred to as SHEAR in the following). Tests with 500 hPa as the upper level were conducted, too, and yielded qualitatively similar results with somewhat weaker links to surface squalls (not shown).

Ideally, the analysis of stability indices would be based on nearby radiosonde data, but the only available station, Pointe Noire (see Fig. 1), only provides 156 profiles, mostly at 1200 UTC, during the three rainy seasons studied here, which is not sufficient for a robust statistical analysis. Comparisons between these data and vertical profiles from the nearest NCEP–NCAR reanalysis grid point showed substantial differences in CAPE and CIN. This is most likely due to the coastal location of the radiosonde station, which makes it very sensitive to

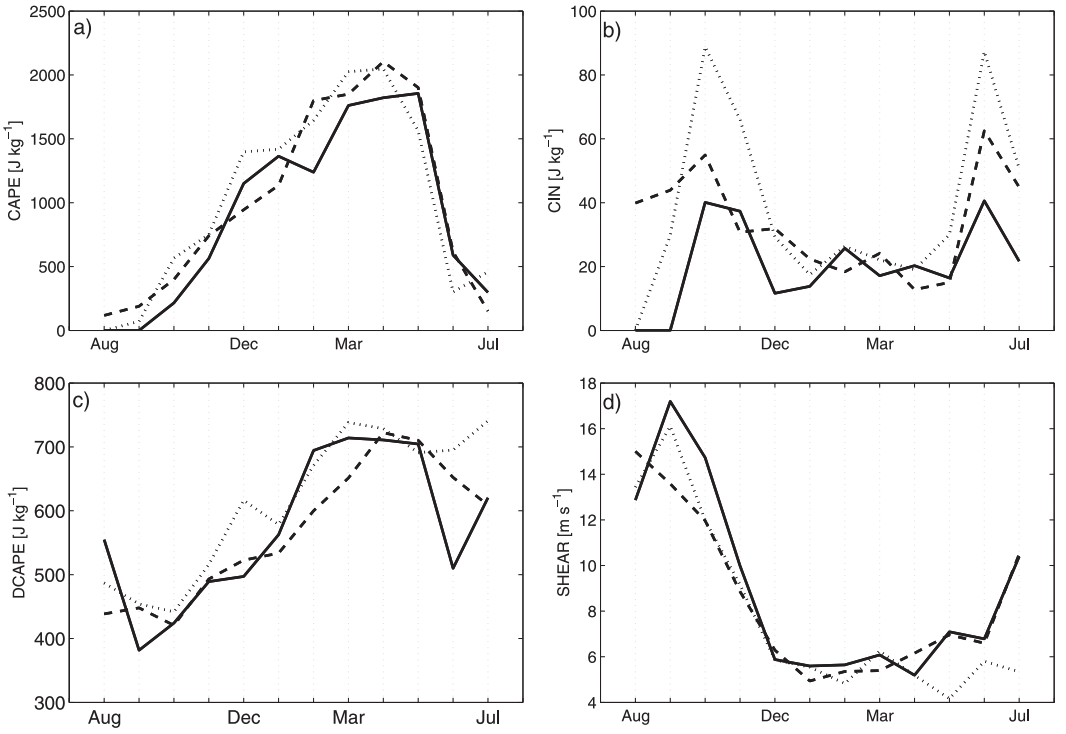

FIG. 6. Monthly means of (a) CAPE, (b) CIN, (c) DCAPE, and (d) SHEAR calculated from 0000 UTC NCEP–NCAR reanalysis data at the nearest grid point (5°S, 12.5°E) for 2006/07 (solid), 2007/08 (dashed), and 2008/09 (dotted).

land–sea-breeze effects and is therefore unrepresentative of conditions over a larger area. It was therefore decided to concentrate on reanalysis data only.

For the NCEP–NCAR reanalysis data, the grid point at 5°S, 12.5°E was chosen, which is very close to the two northern stations. Averages over this and the eight surrounding grid points (2.5°–7.5°S, 10°–15°E) have also been tested on their usefulness for this analysis, but were rejected due to a weaker statistical relationship to the observed squalls. This is most likely related to the generally smaller CAPE over the ocean grid points, fluctuations of which presumably have little influence on the squalls, as the associated convection tends to form over land. As the grid point used here is over land with typical surface pressures around 980 hPa, a mean of the 1000- (extrapolated from lowest model level) and 925-hPa values is used for the hypothetical parcel ascent conducted to determine CAPE and CIN. Tests using the single levels instead generated very low CAPE values in the case of 925 hPa and some rather unrealistic values in the case of 1000 hPa, which probably has to do with problems over extrapolating temperature in a stable nighttime situation.

b. Monthly climatologies

Figure 6 shows monthly averages of the parameters discussed above using 0000 UTC profiles of temperature and moisture from the NCEP–NCAR reanalysis for the three years 2006/07 to 2008/09. Horizontal axes run from August to July in order to center on the rainy season. The time 0000 UTC was chosen to represent conditions for the convection on the following day. The CAPE distribution (Fig. 6a) shows marked annual variations between a maximum of around 2000 J kg^{-1} during the peak of the rainy season (March and April) and very small values during the dry season (July–September). The interannual variability is rather small. One striking exception is the low CAPE values in February of the first rainy season. Not unexpectedly, the annual cycle of squall occurrence (Fig. 2a) largely follows the annual cycle in CAPE, with a gradual increase in both parameters from November to May, followed by a rapid decrease from May to July.

CIN shows a much more complicated annual and interannual pattern of behavior (Fig. 6b). Highest values are typically found just before and right after the rainy season in October–November and June, respectively, with large variations from year to year. During the rainy season itself, values typically range around 20 J kg^{-1} with smaller interannual variability. The low values in August are most likely caused by many days without a discernible LFC level (recall that CIN is set to zero in such cases). This is a general problem of the dry season, when the climatology is a result of such days intermixed

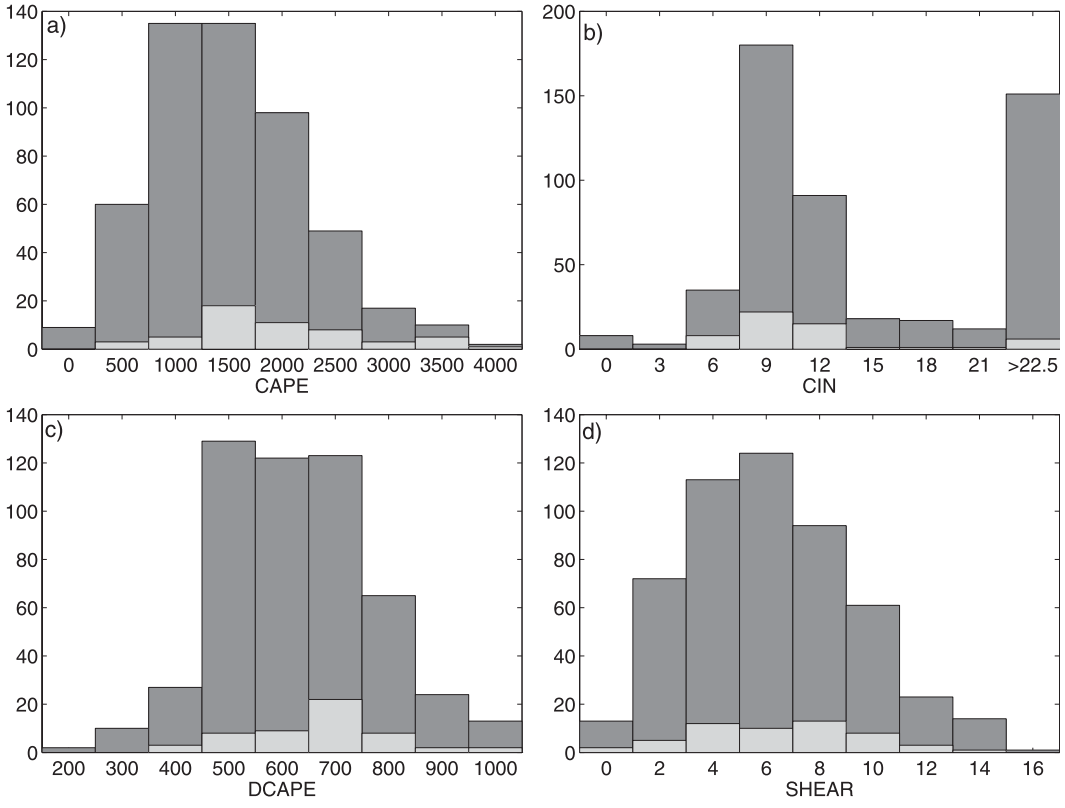

FIG. 7. Frequency histograms of (a) CAPE, (b) CIN, (c) DCAPE, and (d) SHEAR calculated from 0000 UTC NCEP–NCAR reanalysis data at the nearest grid point (5°S, 12.5°E) for each day in the entire period of observation (dark gray) and on squall days (light gray).

with very stable high-CIN conditions. DCAPE largely follows the annual cycle of CAPE, reaching values of more than 700 J kg^{-1} during the main rainy season (Fig. 6c), but high values are sustained beyond the sharp dropoff in CAPE in June with large interannual variations. These values, however, are of little physical relevance, if there is not enough CAPE to sustain convection in the first place. The SHEAR parameter shows its highest values in austral late winter and spring (August–November) in all years (Fig. 6d), which is most likely related to the presence of the Southern Hemispheric African easterly jet during this time of year (Nicholson and Grist 2003; Laing et al. 2011). During the rainy season, SHEAR shows moderate values around 6 m s^{-1} with little year-to-year variations except for very weak shear in May 2009. Repeating this analysis with 1200 UTC instead of 0000 UTC results in a general increase (decrease) of CAPE (CIN) and small changes in DCAPE and SHEAR (not shown).

c. Daily relationship

For potential forecasting purposes it is necessary to establish a relationship between daily values of the stability indices and the occurrence/nonoccurrence of squalls. Taking the annual cycle of squall days into account, it is most sensible to restrict this analysis to the rainy season (November–May), giving a statistical ensemble of 515 days for the investigation period January 2007–March 2009. Figure 7 shows frequency histograms for all four instability indices discussed above for all wet-season days and the 54 identified squall days (10.5% of all days), again based on 0000 UTC profiles from the NCEP–NCAR reanalysis. CAPE, DCAPE, and SHEAR show fairly Gaussian distributions with mean values of 1429 J kg^{-1}, 629 J kg^{-1}, and 7.5 m s^{-1}, respectively. CIN is less than 20 J kg^{-1} for most days with a mean of 11.1 J kg^{-1} and a long tail of the distribution reaching up to 180 J kg^{-1}, which has been summarized into one category in the histogram (Fig. 7b). The latter might be due to the inclusion of the more stable months of November and December, or due to very stable situations after the passage of particularly intense convective systems. Squall days show the expected tendency toward medium to high CAPE and DCAPE, and low CIN, while the SHEAR parameter largely follows the parent distribution (light gray bars in Fig. 7). The χ^2 tests reveal that the statistical likelihood of the squall days to be a random selection from the parent climatology is 0.02% for CAPE, 3% for

TABLE 2. Statistical relationship between squall days and terciles of CIN and CAPE. The basis period of 515 days comprises three wet seasons from January 2007 to March 2009 (see text for more details). Highest number and percentages in the combined categories are given in boldface.

	Total No. of days/No. of squall days (%)			
	CAPE (J kg^{-1})			
CIN (J kg^{-1})	Low (<1109)	Medium (1109–1754)	High (>1754)	Total
High (>18.2)	125/5 (4.0%)	42/3 (7.1%)	8/0 (0.0%)	175/8 (4.6%)
Medium (9.5–18.2)	24/2 (8.3%)	54/6 (11.1%)	93/**15** (16.1%)	171/23 (13.5%)
Low (<9.5)	21/0 (0.0%)	74/10 (13.5%)	74/13 **(17.6%)**	169/23 (13.6%)
Total	170/7 (4.1%)	170/19 (11.2%)	175/28 (16.0%)	515/54 (10.5%)

CIN, 17% for DCAPE, and 89% for SHEAR. In other words, the squall occurrence is almost certainly related to high CAPE and low CIN, while relationships with DCAPE and SHEAR are less clear. This is consistent with the relatively small importance of squall lines (see section 4), which would be expected to be more sensitive to these two parameters.

To make these results more applicable to day-to-day forecasting, the distributions were split into terciles (Tables 2–4). As expected from the discussion above, the strongest relationship is found with CAPE having 4.1% of squall days in the lower, 11.2% in the middle, and 16% in the upper tercile (bottom rows in Tables 2–4). The association of a few cases with very low CAPE is unexpected and might be caused by the increased stability after the passage of an intense system over the grid point, particularly for squalls observed early in the morning. The influence of CIN is most clear for the suppression of convection in the top tercile (>18.2 J kg^{-1}) with only 4.6% of squall occurrences (Table 2). Medium and low CIN values have equal statistical chances of squall days around 13.5%. Combining the CIN and CAPE statistics yields chances of squall occurrence of 17.6% for high CAPE and low CIN and 4% for the opposite combination. This is a powerful result that can be used for operational forecasting for sensitive operations at sea despite the implied high false alarm ratio. The low totals in the top-right and bottom-left cells of Table 2 show that CAPE and CIN are negatively correlated, as discussed in section 5a.

An analogous analysis for CAPE and DCAPE shows a general increase in squall occurrence with DCAPE and even higher squall occurrence for high-CAPE, high-DCAPE situations of 18.7% (Table 3). Recall that the two parameters are usually well correlated, leading to the highest totals in the top-right and bottom-left cells of Table 3. More than a quarter of the (relatively few) situations with high CAPE and SHEAR are associated with squalls (Table 4). Overall, however, the influence of SHEAR on squall occurrence is a little weaker than for DCAPE, which is consistent with the discussion of Fig. 6 above.

A separate investigation for squall lines, microbursts, and unclassified events (see section 4) does not show any systematic difference, partly due to the overall low numbers of events available.

It is interesting to test whether these results can be improved through varying the lead time between the computation of the indices and the observed squalls. A general shift to 1200 UTC of the previous day (instead of 0000 UTC) does not improve the statistics. Mixed statistics using values from both 1200 and 0000 UTC depending on the exact timing of the events are difficult to interpret due to the systematically higher CAPE and lower CIN at 1200 UTC. Using 0000 UTC of the previous day for squalls occurring between 0000 and 0600 or 1200 UTC does not improve the statistics either. This justifies the simple approach of using 0000 UTC as a robust indicator for the likelihood of squall occurrence in the following 24 h.

d. Comparison to ERA-Interim

To test how robust the analyses of stability indices presented in Figs. 6 and 7 and Tables 2–4 are, all relevant

TABLE 3. As Table 2, but for DCAPE and CAPE.

	Total No. of days/No. of squall days (%)			
	CAPE (J kg^{-1})			
DCAPE (J kg^{-1})	Low (<1109)	Medium (1109–1754)	High (>1754)	Total
High (>685)	19/1 (5.3%)	49/7 (14.3%)	107/**20 (18.7%)**	175/28 (16.0%)
Medium (553–685)	56/2 (3.6%)	64/7 (10.9%)	50/6 (12.0%)	170/15 (8.8%)
Low (<553)	95/4 (4.2%)	57/5 (8.8%)	18/2 (11.1%)	170/11 (6.5%)
Total	170/7 (4.1%)	170/19 (11.2%)	175/28 (16.0%)	515/54 (10.5%)

TABLE 4. As in Table 2, but for SHEAR and CAPE.

	Total No. of days/No. of squall days (%)			
	CAPE (J kg^{-1})			
SHEAR (m s^{-1})	Low (<1109)	Medium (1109–1754)	High (>1754)	Total
High (>8.84)	71/3 (4.2%)	57/10 (17.5%)	47/**13** (**27.7**%)	175/26 (14.9%)
Medium (5.69–8.84)	54/2 (3.7%)	62/5 (8.1%)	53/5 (9.7%)	169/12 (7.1%)
Low (<5.69)	45/2 (4.4%)	51/4 (7.8%)	75/10 (13.3%)	171/10 (5.9%)
Total	170/7 (4.1%)	170/19 (11.2%)	175/28 (16.0%)	515/54 (10.5%)

computations were repeated for the same grid point from ERA-Interim using all available pressure levels (spacing of 25 hPa in the lower troposphere). These would not be available to operational forecasts, but can serve as a reference for the coarser NCEP–NCAR data here. The 950-hPa level was chosen as a starting point rather than the 1000–925-hPa average used for NCEP–NCAR. This change, together with the much higher vertical resolution, leads to a systematic decrease in CAPE (maxima during the rainy season ~1300 J kg^{-1}) and increase in CIN (~35 J kg^{-1} during the rainy season) with no major impacts on the annual cycle (not shown; cf. Fig. 6). DCAPE is also systematically reduced in ERA-Interim, particularly in April and May, while SHEAR has a similar annual cycle to that of NCEP–NCAR data, but with somewhat smaller values. The latter result is rather unexpected due to the usage of standard pressure levels in both computations. This suggests some effects of the different model and data assimilation systems that might well affect other parameters, too.

Figure 8 shows histograms for all four parameters in analogy to Fig. 7. Ranges of both CAPE and DCAPE (Figs. 8a and 8c) are clearly reduced with regard to Fig. 7, while the SHEAR distribution (Fig. 8d) is mainly shifted to lower values. With the fixed starting level and the higher vertical resolution, CIN can be determined with much higher accuracy and therefore shows a much broader distribution (Fig. 8b). The χ^2 tests in analogy to section 5c reveal statistical likelihoods of random

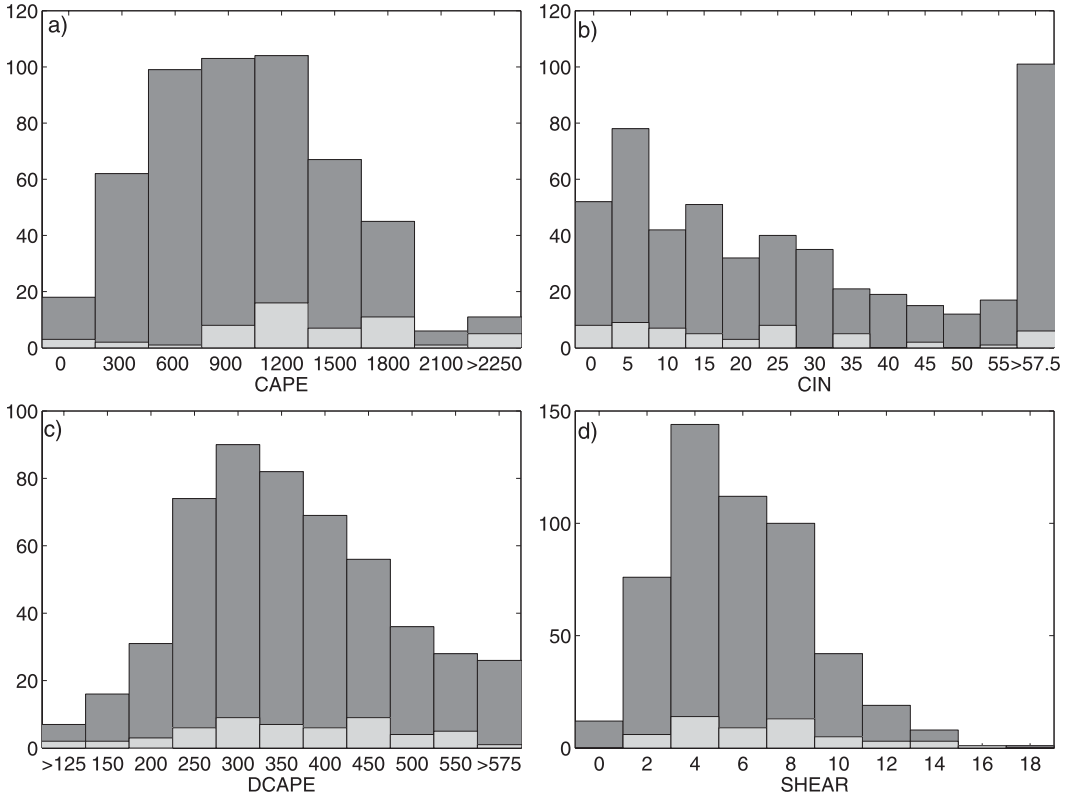

FIG. 8. As in Fig. 7, but for ERA-Interim data. Note that the bin sizes and the values are different from Fig. 7.

selection of 0.0002% for CAPE and 8% for CIN that are not dissimilar to the NCEP–NCAR results, also leading to rather similar values in the tercile analysis presented for NCEP–NCAR in Table 2 (not shown). The values for DCAPE (68%) and SHEAR (5%), however, are not in agreement with the NCEP–NCAR data, which furthers underlines the hypothesized weak physical relationship to the observed squalls discussed above.

6. Conclusions

The Congo Basin and the adjacent equatorial Atlantic belong to the most active, but also to the most poorly observed, convective region on Earth. Surface squalls generated by deep convective systems pose a substantial threat to operations on offshore oil platforms and shipping, which motivates attempts to better understand and forecast this phenomenon. Here, we took advantage of the unique meteorological observations provided by three oil platforms off the coast of Angola to identify convective squall events, compute their climatology, and explore ways of forecasting these. These stations are located at the southwestern edge of the most active region, which is characterized by a sharp dropoff in convective activity near the coast (Jackson et al. 2009).

Not unexpectedly, the climatological analysis reveals a close relationship between the annual cycles of convective activity and rainfall. No squalls are observed during the dry season from June to October. Activity is still weak during November–February, but then increases sharply during the main rainy season (February–May). The diurnal cycle of squall occurrence is relatively flat, but provides some evidence for system propagation from the nearby land and for triggering mechanisms there, such as coastal circulations or orography. However, the available data are far from being sufficient to analyze this aspect any further. Attempts to classify systems are difficult due to the limited amount of information, but suggest a frequent occurrence of microburst-type events, which are generally difficult to forecast, even on the shortest time scales. Mesoscale squall lines appear to only occur at the generally more active northern stations, which are closer to the coast. Again, the limited availability of observations over the continent hampered a clear classification of many events.

Statistical analyses relating daily squall occurrence to instability indices calculated from vertical profiles of temperature and humidity from NCEP–NCAR reanalysis data show an enhanced likelihood of squall occurrence for high CAPE, high DCAPE, and high SHEAR with the influence of the former being by far the most significant. CIN is usually low during the rainy season and therefore mostly influences squall occurrence negatively in situations with exceptionally high values. The statistical relationship with CAPE and CIN are consistent with higher-resolution ERA-Interim data, but those for DCAPE and SHEAR appear less robust.

Overall, the results presented here provide a useful and fairly easy-to-use basis for day-to-day estimates of the chances of squall occurrence in a region where other sources of information are absent. For operational purposes, a combination of climatological information with short-term forecasts is recommended here. The annual and diurnal cycles discussed in this paper can be used for an assessment of the statistical likelihood of the occurrence of a squall on a given day. This information can then be refined through computations of instability indices from vertical profiles taken from the most recent analysis or even from short-term forecasts (not explicitly explored here). Nowcasting based on thermal IR satellite data can further inform decisions, but given that convection is ubiquitous during the rainy season and many details are often obscured by cirrus and anvil clouds, IR imagery alone will most likely generate many false alarms. The fact that many squalls appear to be related to small-scale features such as microbursts suggests that the use of probabilistic approaches would be very useful.

For further refinement of this analysis in the future, longer time series and larger spatial coverage, particularly over the continent, would be desirable. Case studies using numerical models and new satellite data such as *CloudSat* have the potential to advance our understanding of the involved convective dynamics. Furthermore, it would be interesting to explore whether the connection between the active phase of eastward-propagating large-scale waves and the size and intensity of mesoscale convective systems (Nguyen and Duvel 2008; Laing et al. 2011) enhances predictability beyond the very short ranges.

Acknowledgments. The authors thank WAG1 original participants (BP, ChevronTexaco, ConocoPhillips, ExxonMobil, Shell, Statoil, Total, and Woodside) for providing their data. The NOAA–CIRES Climate Diagnostics Center, Boulder, Colorado, is acknowledged for providing NCEP–NCAR reanalysis data for this study, as is the Met Office for providing access to the ECMWF Mars archive. The TRMM data were downloaded from the web-based satellite data system Giovanni run by NASA's Goddard Earth Sciences Data and Information Services Center. Meteosat satellite images were obtained from EUMETSAT. Chris Yetsko (ConocoPhillips, formerly Fugro GEOS), Katie Lean (formerly Oxford University), and Andrew Watson (Fugro GEOS) are acknowledged for contributions to the early stages of this analysis, as is Gourihar Kulkarni for some preliminary work on CAPE

calculations. We are also grateful to three anonymous reviewers whose comments helped to substantially improve an earlier version of this paper.

APPENDIX

Definitions of Stability Indices

Definitions of the stability indices used in section 5 are given in the following:

$$\text{CAPE} = g\int_{z_{\text{LFC}}}^{z_{\text{LNB}}} \frac{T_p - T_e}{T_e}\,dz,$$

$$\text{CIN} = g\int_{z_0}^{z_{\text{LFC}}} \frac{T_p - T_e}{T_e}\,dz, \quad \text{and}$$

$$\text{DCAPE} = g\int_{z_{\max}}^{z_0} \frac{T_p - T_e}{T_e}\,dz$$

where g is the gravitational acceleration; T_p and T_e are the virtual temperatures of an air parcel and the environment, respectively; and z_{LFC}, z_{LNB}, $z_{\max}$, and z_0 are the altitudes of the LFC, the LNB, the level that gives maximum DCAPE, and the surface, respectively (see Emanuel 1994). SHEAR is simply defined as the absolute value of the vector difference between the 700- and 925-hPa pressure levels:

$$\text{SHEAR} = \sqrt{(u_{700} - u_{925})^2 + (v_{700} - v_{925})^2},$$

where u_i and v_i are the zonal–meridional wind components and subscripts give pressure (in hPa).

REFERENCES

Balas, N., S. E. Nicholson, and D. Klotter, 2007: The relationship of rainfall variability in west central Africa to sea-surface temperature fluctuations. *Int. J. Climatol.,* **27,** 1335–1349.

Bolton, D., 1980: The computation of equivalent potential temperature. *Mon. Wea. Rev.,* **108,** 1046–1053.

Chong, M., P. Amayenc, G. Scialom, and J. Testud, 1987: A tropical squall line observed during the COPT 81 experiment in West Africa. Part I: Kinematic structure inferred from dual-Doppler radar data. *Mon. Wea. Rev.,* **115,** 670–694.

Christian, H. J., and Coauthors, 2003: Global frequency and distribution of lightning as observed from space by the Optical Transient Detector. *J. Geophys. Res.,* **108,** 4005, doi:10.1029/2002JD002347.

Dee, D. P., and Coauthors, 2011: The ERA-Interim reanalysis: Configuration and performance of the data assimilation system. *Quart. J. Roy. Meteor. Soc.,* **137,** 553–597.

Doswell, C. A., III, 2001: *Severe Convective Storms—An Overview. Meteor. Monogr.,* No. 50, Amer. Meteor. Soc., 561 pp.

Emanuel, K., 1994: *Atmospheric Convection*. Oxford University Press, 580 pp.

Houze, R. A., Jr., 1977: Structure and dynamics of a tropical squall-line system. *Mon. Wea. Rev.,* **105,** 1540–1567.

Huffman, G. J., R. F. Adler, S. Curtis, D. T. Bolvin, and E. J. Nelkin, 2007: Global rainfall analyses at monthly and 3-hr time scales. *Measuring Precipitation from Space: EURAINSAT and the Future,* V. Levizzani, P. Bauer, and F. J. Turk, Eds., Springer Verlag, 291–306.

Jackson, B., S. E. Nicholson, and D. Klotter, 2009: Mesoscale convective systems over western equatorial Africa and their relationship to large-scale circulation. *Mon. Wea. Rev.,* **137,** 1272–1294.

Jeans, G., and R. Johnson, 2011: The WAG Platform Structural Effects Study. *Proc. 30th Int. Conf. on Ocean, Offshore and Arctic,* Rotterdam, Netherlands, ASME, 835–847, doi:10.1115/OMAE2011-50138.

Jury, M. R., E. Matari, and M. Matitu, 2009: Equatorial African climate teleconnections. *Theor. Appl. Climatol.,* **95,** 407–416.

Kalnay, E., and Coauthors, 1996: The NCEP/NCAR 40-Year Reanalysis Project. *Bull. Amer. Meteor. Soc.,* **77,** 437–470.

Knupp, K. R., and W. R. Cotton, 1985: Convective cloud downdraft structure—An interpretive survey. *Rev. Geophys.,* **23,** 183–215.

Laing, A. G., and J. M. Fritsch, 1993: Mesoscale convective complexes in Africa. *Mon. Wea. Rev.,* **121,** 2254–2263.

——, R. E. Carbone, and V. Levizzani, 2011: Cycles and propagation of deep convection over equatorial Africa. *Mon. Wea. Rev.,* **139,** 2832–2853.

Leroux, M., 2001: *The Meteorology and Climate of Tropical Africa*. Springer, 548 pp.

Marsham, J. H., D. J. Parker, C. M. Grams, C. M. Taylor, and J. M. Haywood, 2008: Uplift of Saharan dust south of the intertropical discontinuity. *J. Geophys. Res.,* **113,** D21102, doi:10.1029/2008JD009844.

McCollum, J. R., A. Gruber, and M. B. Ba, 2000: Discrepancy between gauges and satellite estimates of rainfall in equatorial Africa. *J. Appl. Meteor.,* **39,** 666–679.

Mori, S., H. Jun-Ichi, Y. I. Tauhid, and M. D. Yamanaka, 2004: Diurnal land–sea rainfall peak migration over Sumatera Island, Indonesian Maritime Continent, observed by TRMM satellite and intensive rawinsonde soundings. *Mon. Wea. Rev.,* **132,** 2021–2039.

Müller, C. K., J. W. Wilson, and N. A. Crook, 1993: The utility of sounding and mesonet data to nowcast thunderstorm initiation. *Wea. Forecasting,* **8,** 132–146.

Negri, A. J., T. L. Bell, and L. Xu, 2002: Sampling of the diurnal cycle of precipitation using TRMM. *J. Atmos. Oceanic Technol.,* **19,** 1333–1344.

Nguyen, H., and J.-P. Duvel, 2008: Synoptic wave perturbations and convective systems over equatorial Africa. *J. Climate,* **21,** 6372–6388.

Nicholson, S. E., and J. P. Grist, 2003: On the seasonal evolution of atmospheric circulation over West Africa and equatorial Africa. *J. Climate,* **16,** 1013–1030.

Proctor, F. H., 1988: Numerical simulations of an isolated microburst. Part I: Dynamics and structure. *J. Atmos. Sci.,* **45,** 3137–3160.

——, 1989: Numerical simulations of an isolated microburst. Part II: Sensitivity experiments. *J. Atmos. Sci.,* **46,** 2143–2165.

Rasmussen, E. N., and D. O. Blanchard, 1998: A baseline climatology of sounding-derived supercell and tornado forecast parameters. *Wea. Forecasting,* **13,** 1148–1164.

Savvidou, K., A. Orphanou, D. Charalambous, P. Lingis, and S. Michaelides, 2010: A statistical analysis of sounding derived indices and parameters for extreme and non-extreme thunderstorms events over Cyprus. *Adv. Geosci.,* **23,** 79–85.

Toracinta, E. R., and E. J. Zipser, 2001: Lightning and SSM/I-ice-scattering mesoscale convective systems in the global tropics. *J. Appl. Meteor.,* **40,** 983–1002.

Wakimoto, R. M., 2001: Convectively driven high wind events. *Severe Convective Storms—An Overview, Meteor. Monogr.,* No. 50, Amer. Meteor. Soc., 255–298.

Williams, E. R., and G. Sátori, 2004: Lightning, thermodynamic and hydrological comparison of the two tropical continental chimneys. *J. Atmos. Sol. Terr. Phys.,* **66,** 1213–1231.

WMO, 1962: Supplement to the WMO publication No. 122.RP.50 abridged final report of the third session of the Commission for Synoptic Meteorology. World Meteorological Organization, 228 pp.

Yang, G. Y., and J. Slingo, 2001: The diurnal cycle in the tropics. *Mon. Wea. Rev.,* **129,** 784–801.

Zipser, E. J., 1977: Mesoscale and convective-scale downdrafts as distinct components of squall-line structure. *Mon. Wea. Rev.,* **105,** 1568–1589.